Note: This is an in-press pre-proof peer-reviewed draft of the journal article:

Lennert de Ruiter, Kathryn Rankin, Martin Browne, Adam Briscoe, Dennis Janssen, Nico Verdonschot (2021) "Decreased stress shielding with a PEEK femoral total knee prosthesis measured in validated computational models". Journal of Biomechanics 110270,

ISSN 0021-9290

DOI: https://doi.org/10.1016/j.jbiomech.2021.110270

Available online 28th January 2021 at:
http://www.sciencedirect.com/science/article/pii/S0021929021000506

Manuscript

Decreased stress shielding with a PEEK femoral total knee prosthesis measured in validated computational models

Original Article

Lennert de Ruiter
Orthopaedic Research Lab, Radboud University Medical Center Nijmegen, The Netherlands

Kathryn Rankin
Bioengineering Science Research Group, Faculty of Engineering and Physical Sciences, University of Southampton, Southampton, UK

Martin Browne
Bioengineering Science Research Group, Faculty of Engineering and Physical Sciences, University of Southampton, Southampton, UK

Adam Briscoe
Invibio Ltd., Lancashire, UK

Dennis Janssen (corresponding author)
Orthopaedic Research Lab
Department of Orthopaedics
Radboud Institute for Health Sciences
Radboud University Medical Center Nijmegen
P.O. Box 9101
6500 HB Nijmegen
The Netherlands
T: +31 (0)24 36 16959
E: dennis.janssen@radboudumc.nl

Nico Verdonschot
Orthopaedic Research Lab, Radboud University Medical Center Nijmegen, The Netherlands
Institute of Biomedical Technology, University of Twente, Enschede, The Netherlands

Keywords: total knee arthroplasty, polyetheretherketone, stress shielding, finite element simulation, digital image correlation

Word count: 3282

ABSTRACT

Due to their high stiffness, metal femoral implants in total knee arthroplasty may cause stress shielding of the peri-prosthetic bone, which can lead to loss of bone stock. Using a polymer (PEEK) femoral implant reduces the stiffness mismatch between implant and bone, and therefore has the potential to decrease strain shielding. The goal of the current study was to evaluate this potential benefit of PEEK femoral components in cadaveric experiments. Cadaveric femurs were loaded in a materials testing device, while a 3-D digital image correlation set-up captured strains on the surface of the intact femurs and femurs implanted with PEEK and CoCr components. These experimental results were used to validate specimen-specific finite element models, which subsequently were used to assess the effect of metal and PEEK femoral components on the bone strain energy density. The finite element models showed strain maps that were highly comparable to the experimental measurements. The PEEK implant increased strain energy density, relative to the preoperative bone and compared to CoCr. This was most pronounced in the regions directly under the implant and near load contact sites. These data confirm the hypothesis that a PEEK femoral implant can reduce peri-prosthetic stress shielding.

INTRODUCTION

Total knee arthroplasty is one of the most successful interventions in orthopaedic surgery for treatment of patients suffering from degenerative knee joints, with impressive survival rates [AOANJRR, 2019]. Despite its success, there is still a small number of cases that require revision for aseptic loosening, which is why there is an ongoing drive for development of new implant systems and materials. Before clinical introduction, these new systems should be subjected to extensive pre-clinical evaluation to determine its potential benefits and risks.

Recently, the effect of a polyetheretherketone (PEEK) femoral total knee arthroplasty TKA component was studied in computational analyses (de Ruiter et al., 2017a, 2017b). Those studies demonstrated that a PEEK knee implant may improve the periprosthetic bone remodelling stimulus. During a squatting exercise the PEEK material reduced the stress shielding by 55 percent points compared to a CoCr device. A study by Rankin et al. demonstrated this potential in in vitro experiments with a bone-analogue model (Rankin et al., 2016). Both the computational and in vitro studies confirmed the hypothesis that a more compliant material can distribute forces more physiologically than when using a stiff metal implant.

In TKA, change in mechanical loading of the bone is the main stimulus driving remodelling and periprosthetic bone density changes, which is influenced by the relatively stiff implant materials being used, such as Cobalt-Chromium (CoCr) (Carter et al., 1987; Frost, 1964; Huiskes et al., 1987; Kummer, 1972; Lenthe et al., 2002, 1997; Mintzer et al., 1990; Wolff, 1869). A reduced bone stimulus may lead to resorption and osteopenia, which in turn increases the risk of periprosthetic bone fractures (Järvenpää et al., 2014; Lavernia et al., 2014; Mintzer et al., 1990). At other locations the stiff TKA materials may generate high stresses in the underlying bone, which further increases the fracture risk (de Ruiter et al., 2017b, 2017a). These fractures occur in up to 5% of TKA patients, depending on service time, and are often the result of trauma, in combination with a weakened bone stock (Canton et al., 2017; Schroer et al., 2013; Seki et al., 1999). Therefore, alternative, more compliant materials that have the potential to reduce stress shielding have been considered for femoral TKA components, such as polyacetal implants that were evaluated in a clinical trial (Moore et al., 1998).

The in vitro study as performed by Rankin *et al. (2016)* used digital image correlation (DIC) to measure surface strains on the cortical surface during loads equivalent to level gait. This technique provides a robust quantification of small two- or three-dimensional displacements and strains (Dickinson et al., 2011). However, it can only measure on visible surfaces and, as such, can only identify stress shielding at the cortical surface. Finite element (FE) modelling does have the capability to determine internal bone strains (de Ruiter et al., 2017b, 2017a). In the current study, experimental measurements using DIC were therefore combined with FE modelling to investigate the effect of femoral TKA with PEEK and CoCr components on peri-prosthetic bone strains.

We hypothesized that a PEEK femoral component would cause a bone strain distribution that more closely resembles the intact situation compared to a reconstruction with a CoCr component.

MATERIALS AND METHODS

The current study combined experimental DIC analysis, to quantify the change in surface bone strains following reconstruction with either a PEEK or a CoCr component, with FE analyses for evaluation of the surface and internal bone strain changes.

Study design

Experiments were conducted with three pairs of human cadaveric femurs. DIC strain measurements were first taken from the intact femurs to serve as a control after implantation. Left femurs were implanted with PEEK implants, and right femurs with CoCr implants, assuming similarity in geometry and mechanical properties of the bones (Pierre et al., 2010). The PEEK and CoCr implants had the exact same geometry, with the difference that the cement pockets of the PEEK components were equipped with ribs to provide additional fixation with the cement. Comparison of the intact and post-implantation situations illustrated the effect of TKA on the changes in load transfer, while comparing between the left and right reconstructed femurs provided information on the effect of implant material. Specimen-specific FE models were created

and validated against the experimental surface strains, and subsequently used to investigate the internal periprosthetic bone strain distribution.

Specimen preparation

Six fresh-frozen human cadaveric femurs (three pairs, female donors, 76-83 years) were CT-scanned to exclude the presence of foreign materials, or signs of pathology or severe osteoporosis. The femurs were dissected distally, thawed at room temperature and cleaned from soft tissues. Special care was given to the lateral epicondylar region to facilitate DIC measurements. A polyurethane resin mould (Smooth-Cast 60D, Smooth-On Inc. USA), potted in polymethylmethacrylate (PMMA), was created from the femoral articulating surface to form a custom load applicator for the intact femur measurement. Next, the intercondylar entry point into the intramedullary canal was drilled for placement of the surgical tools. Each specimen was then potted in PMMA 100 mm proximally from the distal femur. To ensure a reproducible load application between the intact and implanted femurs, femoral alignment was controlled by inserting the surgical alignment tool into the intramedullary canal, which subsequently was equipped with a customized planar spirit level. This ensured horizontal alignment of the (future) distal cut and resulted in the correct flexion angle during potting. After curing of the bone cement a Perspex rod was inserted into the intramedullary canal to keep it open and visible on the computed tomography (CT) scans that followed. All specimens were then submerged in a water-basin to simulate peripheral soft tissues, and were CT-scanned (530 mA, 120 kV, 0.5x0.5 mm in-plane resolution, 1.0 mm slice thickness, Siemens Somatom Sensation 64, Siemens AG, Germany) along with a calibration phantom (Image Analysis Inc., Columbia, KY, USA) (Carballido-Gamio et al., 2015; Cuppone et al., 2004; Keyak et al., 2005; Keyak and Falkinstein, 2003; Lenaerts and van Lenthe, 2009). After scanning all specimens were refrozen.

Experimental procedure

Before testing, specimens were thawed at room temperature for at least 12 hours. After drying in ambient air, the surface was coated with matt white spray paint (Plastikote Ltd, UK). Once dry, a matt black speckle pattern was applied onto the white surface by an experienced DIC operator. Then, the specimen was placed

in the unidirectional servo-hydraulic loading apparatus with a 15kN load cell (MTS45820, MTS Systems Corp., USA) (Figure 1). The specimens-specific polyurethane mould was positioned onto the femoral cartilage, aligned using a laser spirit level, and then potted in PMMA for fixation to the loading apparatus. After curing of the PMMA and seating of the load applicator onto the specimen, ambient and focal light sources were positioned to obtain optimal lighting of the specimen (Figure 1). The uniaxial compression load for the specimens was not predefined as a fixed value, to avoid femoral fractures. Alternatively, the specimen-specific load was determined using the left femur by first measuring the unloaded baseline noise in the DIC setup, after which the femoral load was increased incrementally until a 10:1 signal-to-noise ratio (SNR) was achieved. A 10:1 SNR provides good accuracy of the captured data, accounts for potential noise increase and reduces any measurement error to an acceptable level. The resulting loads were 3.5 kN, 2.5 kN and 3.5 kN for specimens 1, 2 and 3, respectively. These loads were then applied to both the left and right femurs. The load applicator allowed for free translations in the horizontal plane and free varus/valgus rotations, while other degrees of freedom were constrained. Six cycles of loading/unloading were executed. Of each loaded and unloaded state six DIC image arrays were captured.

Following the intact femur measurements, either a CoCr (Maxx Freedom Knee) or PEEK (adopted from Maxx Freedom Knee) implant was cemented (Palacos R, Palamix system, Heraeus Medical GmbH, Germany) onto the femur according to surgical guidelines. After implantation, one hour was allowed for cement curing, after which the specimen was placed back into the testing rig and the experimental procedure as described above was repeated.

Digital image correlation

A dual-camera DIC setup using Sigma 105mm lenses was used (Limess GmbH, 2 megapixel) to capture 3-D femur strain data (Figure 1). Prior to a measurement series, the corresponding rigid DIC-calibration tool (12 x 9 grid of 5 mm targets) was used to calibrate the position of the cameras relative to one another via triangulation to define the 3D coordinate system for the bone surface. The camera setup was placed at approximately one meter from the specimens for optimal focal depth, with a relative pan angle of 10 degrees for 3-D capturing. As the region of interest (ROI – Figure 2) must be visible for both cameras, higher angles

could lead to loss of field of view. Images were captured using Vic3D software (Correlated Solutions Inc., Irmo, SC, USA). Lighting was arranged such that maximal contrast was reached while avoiding pixel saturation. The Vic3D software indicated when image conditions were sufficient for accurate analysis, indicating a suitable spread in the grey scale histogram (i.e. not oversaturated, nor too dark), which was obtained by adjusting lighting. This baseline assessment was performed on unloaded specimens and revealed if the agreement between the two cameras was adequate for the experimental procedure. The same interrogation area was used across each bone surface with a subset size of 41 × 41 pixels, and a step size of 7 pixels, with normalised sum of square differences (NSSD) correlation criterion. The strain resolution of the system was 30±38 μstrain with similar geometry specimens under ideal conditions (Rankin et al., 2016).

Finite element models

Geometry

FE models were based on the CT scans of the intact, potted femurs. CT-scans were exported with a bone filter and with a soft tissue filter for better visibility of the femoral cartilage. The femurs were segmented based on the bone scan, while the differences between scans in the condylar area were assumed to represent the cartilage layer, which were then added to the femur. A surface representation was created using Mimics 14 (Materialise, Leuven, Belgium), which was then used to create a solid mesh (Patran, MSC Software, Newport Beach, CA, USA). The models were meshed with tetrahedral elements with an average edge length of 2 millimetres, based on previous FE studies with a similar loading configuration (de Ruiter et al., 2017b). The PMMA fixation was segmented as a vertical reference, while the Perspex rod was segmented as a reference for the distal cut. Two pins of the distal femoral cutting guide left indents in the femur during implantation, which were identified on the CT scans and used as reference for the final alignment of the distal cut. The custom load applicators were digitized by a white-light scanner (Creaform Go!SCAN 3D 2012). The bearing surface mesh was positioned on the femoral condylar cartilage via a customized positioning algorithm with the constraints of horizontal alignment and varus/valgus rotation, according to the experimental degrees of freedom. The placement was then compared to anteroposterior and mediolateral pictures taken during the experiment to verify the positioning in the models.

Material properties

To assign material properties to the femurs, the Hounsfield units were first converted to bone mineral density (BMD) using the calibration phantom. The BMD was subsequently used to calculate the local Young's modulus for the femurs using equations by Keyak et al. (2005) (Keyak et al., 2005). All other materials were given homogeneous material properties as provided by manufacturers (Table 1). The comparison between DIC strain data and FE strain data on the lateral epicondylar surface was facilitated by connecting zero-thickness surface elements to the tetrahedrons' vertices on the surface in the region of interest, which was meshed with a higher density (average edge length of 1 mm). These surface elements were given a near-zero stiffness to ensure they followed the deformation of the underlying bone elements and provided strains metrics identical to the DIC measurements.

Table 1. Material properties.

Material	Young's modulus (MPa)	Poisson's ratio
CoCr	210,000	0.3
PEEK-Optima®	3,700	0.362
Polyurethane	800	0.3
PMMA	2,866	0.3
Femur	1-20,000	0.3

Loading

The experimental load was replicated via one node connected to the load applicator via stiff springs, simulating the experimental load transfer and degrees of freedom. The models were fixed at the elements representing the PMMA pot.

Outcome measures

Experimental surface strain comparison and FE strain validation

The surface strain measured by the DIC software was a Von Mises strain for zero-thickness surfaces as defined by Equation 1. The equation was implemented in the ROI surface elements of the FE models for direct DIC/FE comparison. DIC data was averaged twice: first, over the image arrays within one load instance, and second the mean over the six load instances was taken. The resulting strain map was assessed qualitatively for patterns, and quantitatively by analysing the strain distribution in the DIC region in 500-microstrain intervals. These were subsequently compared to the FE strain map, providing a measure for the accuracy of the FE models.

$$\varepsilon_{vm} = \sqrt{\varepsilon_1{}^2 - \varepsilon_1\varepsilon_2 + \varepsilon_2{}^2} \qquad \textbf{Equation 1.}$$

In this equation, ε_1 and ε_2 represent the orthogonal strains in the horizontal and vertical directions, respectively.

Volumetric strain (shielding) assessment

Strain energy density (SED) was calculated in the FE models as a measure for stress shielding in the in the periprosthetic femur. SED has been described in literature as the stimulus for bone remodelling (Carter et al., 1987; Huiskes et al., 1987), with a decrease in SED causing loss of bone mass. A comparison between the intact and implanted femur is therefore required to predict postoperative periprosthetic bone changes. To this end, the SED data of the intact femur measurements were subtracted from the CoCr and PEEK reconstructions at each integration point in the periprosthetic volume. The integration point data were then multiplied by their element volume and summed to yield the total strain energy in all five periprosthetic regions of interest (ROI). The ROIs were determined in the sagittal view, according to representations in literature (Lavernia et al., 2014; Lenthe et al., 1997). The condylar ROIs were split for lateral and medial condyle, effectively creating 7 ROIs (Figure 5).

RESULTS

Experimental observations

During the experiment events were observed that were not according to protocol. During capturing of the DIC images, on several occasions one or two out of six image recordings were unsuitable for measurement, leaving 4 or 5 strain maps for strain averaging. Secondly, the load applicator for one pair of implanted femurs (specimen 2) was slightly undersized, which was resolved by moving the load applicator to ensure optimal lateral seating, where DIC data was being recorded. The shift of the load applicator was implemented correspondingly in the FE models of these femurs, based on images of the adjusted set-up, while the loading configuration was unchanged.

Experimental surface strain comparison

The largest strain values were measured in the distal femur, in line with the principal loading direction, with maximum values ranging from 2090 µstrain (Specimen 1, implanted, right) to 4760 µstrain (Specimen 3, intact, left) (Figure 3). Strain distributions were similar between left and right leg intact femurs, confirming similarity between contralateral specimens.

Once implanted, the epicondylar surface strains generally decreased, suggesting stress shielding in both reconstructions. The strain decrease was larger with a CoCr implant than with a PEEK component, which was particularly obvious in specimens 1 and 2, and more subtly in specimen 3. Frequency plots of the surface microstrains showed a higher peak in the low-strain region for the implanted specimens, which in case for specimens 1 and 2 were more pronounced for the CoCr reconstructions (Figure 4). For the larger strain regions, typically, the curves for the intact specimens were slightly above the implanted specimens, indicating strain-shielding for both implant types.

In general, the FE simulations showed good agreement with the experimental strain patterns (Figure 3) and magnitudes (Figure 4), and thus provided a satisfactory validation of the models. Exceptions were the intact right (PEEK) FE models of specimens 1 and 2, which showed a similar distribution but generally lower strain values, which was also reflected in the strain frequency plots (Figure 4).

Volumetric strain (shielding) assessment

For all specimens PEEK led to an overall increase in SED compared to the intact cases, whereas for CoCr a decrease was seen in specimen 1 and slight increases in specimens 2 and 3 (Figure 5). For specimens 1 and 2, the increase in SED in the PEEK reconstructions was most pronounced distally (ROI 5), while in specimen 3 this increase was also seen more proximally (ROI 3). Stress shielding was observed in the PEEK reconstructions of specimens 2 and 3 in the anterodistal area (ROI 1), but to a lesser extent than CoCr. CoCr reconstructions always showed lower SED values ROIs 1 and 5. The difference with intact was smaller in the medial regions of ROI 5 than in the lateral regions. Only small differences were seen between PEEK and CoCr reconstructions in the proximal regions (ROI 2 and 3). In the posterior region (ROI 4) the differences between intact and implanted were small for both implant materials.

DISCUSSION

We hypothesized a PEEK femoral component would cause a strain distribution more closely resembling the intact situation compared to a reconstruction with a CoCr component. Our DIC results on the surface strains indeed confirmed this hypothesis. Similarly, internal strain energy density distributions calculated by FE were more similar to the intact femurs with PEEK in regions 1 and 5.

From a qualitative perspective, the FE models displayed surface strain distributions that were very similar to the experimental DIC measurements. The largest strain mismatch was observed in the right intact femur of specimen 2. Although the patterns were similar, the magnitude of the DIC strain was substantially larger. This may have been caused by the experimental loading configuration, in which the varus/valgus rotation that was allowed may have led to a load imbalance, with an increased portion of the load acting on the lateral femur. This was confirmed in additional FE simulations in which, in addition to the change in the positioning of the load applicator, this assumed load imbalance was incorporated. The results of that simulation showed a similar increase in strain in the lateral femur.

Reduced stress shielding was seen in the PEEK reconstructions, particularly due to a more favorable strain energy distribution in the (antero)distal area. Conversely, stress shielding was always observed with a CoCr implant in this region. Interestingly, the PEEK implant showed an increase in strain energy density, leading to the expectation for increased bone formation. Although it is desirable to increase bone quality in generally osteopenic bones, an increase in bone loading may also increase the risk of periprosthetic fractures. The current FE results show the same trend as previous studies where the bone remodeling stimulus of a PEEK femoral TKA was analyzed (de Ruiter et al., 2017b, 2017a; Rankin et al., 2016). Both during simulated level gait (de Ruiter et al., 2017b) and squatting (de Ruiter et al., 2017a), a clear reduction in stress shielding was seen with a PEEK component, although these studies only included a single bone geometry and simplified bone material properties. Experimental data on standardized analogue femurs with PEEK and CoCr femoral prostheses demonstrated a similar trend (Rankin et al., 2016).

TKA is a successful orthopaedic intervention, as demonstrated in large clinical studies and implant registries. In contrast, a significant number of knee patients is not satisfied after surgery, with TKA scoring lower patient satisfaction scores than patients undergoing total hip arthroplasty. While this obviously is a multifactorial problem, part of the answer to the low satisfaction rates may lie in the use of alternative materials such as PEEK, which more closely replicates the characteristics of the tissue that is being replaced, in terms of density, thermal conductivity, and as investigated in the current study, stiffness. In addition, a PEEK component may be of interest for patients suffering from metal ion sensitivity. By combining a PEEK femoral component with an all-poly tibial tray, an all-poly TKA solution can be achieved for these patients.

Apart from the potential benefits of a PEEK femoral component, the introduction of new technology also comes with potential risks. While not investigated in the current study, the use a PEEK femoral implant has implications for the stresses acting on the implant-cement interface and the cement mantle. Previous studies using experimental testing and computational modelling indicated a reduction in initial fixation strength of a PEEK femoral relative to an exact CoCr copy, which led to the addition of fixation ribs at the implant-cement interface to improve this strength to about 2.5 kN (de Ruiter et al., 2017c). FE models furthermore demonstrated the effect of a PEEK component on the cement and interface stress distributions under gait (de Ruiter et al., 2017b) and squat (de Ruiter et al., 2017a) loads. These simulations indicated

lower stresses in the implant and cement, but higher stresses at the implant-cement interface. Similarly, analysis long-term loaded femoral components demonstrated more initial gaps at the implant-cement interface, but no differences between PEEK and CoCr reconstructions after 10 million loading cycles (de Ruiter et al., 2020). In addition, similar amounts of cement damage were found at 10 million cycles. While these pre-clinical findings provide evidence for clinical application, the clinical value a PEEK femoral component can only be demonstrated in a clinical trial.

This study has several limitations with regard to the design, statistics and analysis. First, only three pairs of femurs were used for testing and analysis. Cadaver studies are rarely sizable enough to establish statistical support for a conclusion due to, amongst others, variability in specimen size and bone quality (Pierre et al., 2010), and limited specimen availability. Consequently, the data that were obtained in this small-sample study were intended to support hypothesized trends, build confidence and improve on previously generated data. The FE models that were created during this study proved to be robust and an accurate representation of the experiment, generating the desired confidence.

Only a single loading configuration was analysed in the experimental set-up, whereas load variations could have revealed difference in the femoral strain, as shown in our previous FE simulations of PEEK and CoCr reconstructions (de Ruiter et al., 2017b, 2017a).

Considering the FE models, an ideal bond was assumed between the cement and bone, and as such did not incorporate the interdigitated region of cement and bone. This may have affected the prediction of the internal SED distribution in this region, although the extent of cement penetration may be relatively small compared to the size of the regions of interest that were defined.

Conclusion

This cadaveric study demonstrates the potential for PEEK femoral components to reduce periprosthetic bone strains to more physiological levels when compared to CoCr.

Acknowledgements

This study was funded by Invibio Ltd, Lancashire, UK. Invibio Ltd was not involved in the study design, collection, analysis and interpretation of data.

Conflict of interest statement

A.B. is a paid employee of Invibio Ltd. and had a role in the study design and review of the manuscript. M.B. has received research funding support from Invibio Ltd. N.V. is a consultant to Invibio Ltd. The other authors declare no conflict of interest. The funders had no role in the design of the study; in the collection, analyses, or interpretation of data.

REFERENCES

Australian Orthopaedic Association National Joint Replacement Registry (AOANJRR). Hip, Knee & Shoulder Arthroplasty: 2019 Annual Report. Adelaide: AOA, 2019.

Canton, G., Ratti, C., Fattori, R., Hoxhaj, B.B., Murena, L., 2017. Periprosthetic knee fractures. A review of epidemiology, risk factors, diagnosis, management and outcome. Acta Biomed. 88, 118–128. https://doi.org/10.23750/abm.v88i2

Carballido-Gamio, J., Bonaretti, S., Saeed, I., Harnish, R., Recker, R., Burghardt, A.J., Keyak, J.H., Harris, T., Khosla, S., Lang, T.F., 2015. Automatic multi-parametric quantification of the proximal femur with quantitative computed tomography. Quant. Imaging Med. Surg. 5, 552–568. https://doi.org/10.3978/j.issn.2223-4292.2015.08.02

Carter, D.R., Fyhrie, D.P., Whalen, R.T., 1987. Trabecular bone density and loading history: regulation of connective tissue biology by mechanical energy. J. Biomech. 20, 785–794.

Cuppone, M., Seedhom, B.B., Berry, E., Ostell, A.E., 2004. The Longitudinal Young's Modulus of Cortical Bone in the Midshaft of Human Femur and its Correlation with CT Scanning Data. Calcif. Tissue Int. 74, 302–309.

de Ruiter, L., Janssen, D., Briscoe, A., Verdonschot, N., 2017a. The mechanical response of a polyetheretherketone femoral knee implant under a deep squatting loading condition. Proc. Inst.

Mech. Eng. H. 231.

de Ruiter, L., Janssen, D., Briscoe, A., Verdonschot, N., 2017b. A preclinical numerical assessment of a polyetheretherketone femoral component in total knee arthroplasty during gait. J. Exp. Orthop. 4, 3.

de Ruiter, L., Janssen, D., Briscoe, A., Verdonschot, N., 2017c. Fixation strength of a polyetheretherketone femoral component in total knee arthroplasty. Med. Eng. Phys. 49, 157–162.

de Ruiter, L., Cowie R.M., Jennings L.M., Briscoe, A., Janssen, D., Verdonschot, N., 2020. The Effects of Cyclic Loading and Motion on the Implant–Cement Interface and Cement Mantle of PEEK and Cobalt–Chromium Femoral Total Knee Arthroplasty Implants: A Preliminary Study. Materials 13, 3323.

Dickinson, A., Taylor, A., Ozturk, H., Browne, M., 2011. Experimental validation of a finite element model of the proximal femur using digital image correlation and a composite bone model. J. Biomed. Eng. 133, 014504.

Frost, H., 1964. The Laws of Bone Structure. Charles C. Thomas, Springfield, IL.

Huiskes, R., Weinans, H., Grootenboer, H.J., Dalstra, M., Fudala, B., Slooff, T.J., 1987. Adaptive Bone-Remodeling Theory Applied to Prosthetic-Design Analysis. J. Biomech. 20, 1135–1150.

Järvenpää, J., Soininvaara, T., Kettunen, J., Miettinen, H., Kröger, H., 2014. Changes in bone mineral density of the distal femur after total knee arthroplasty: a 7-year DEXA follow-up comparing results between obese and nonobese patients. Knee 21, 232–5.

Keyak, J.H., Falkinstein, Y., 2003. Comparison of in situ and in vitro CT scan-based finite element model predictions of proximal femoral fracture load. Med. Eng. Phys. 25, 781–787. https://doi.org/10.1016/S1350-4533(03)00081-X

Keyak, J.H., Kaneko, T.S., Tehranzadeh, J., Skinner, H.B., 2005. Predicting Proximal Femoral Strength Using Structural Engineering Models. Clin. Orthop. Relat. Res. 219–228. https://doi.org/10.1097/01.blo.0000164400.37905.22

Kummer, B., 1972. Biomechanics of bone: Mechanical properties, functional structure, and functional adaptation., in: Fung, Y., Perrone, N., Anliker, M. (Eds.), Biomechanics: Its Foundations and Objectives. Prentice-Hall, Englewood Cliffs, NJ, p. 237:271.

Lavernia, C.J., Rodriguez, J. a, Iacobelli, D. a, Hungerford, D.S., Krackow, K. a, 2014. Bone mineral density of

353 the femur in autopsy retrieved total knee arthroplasties. J. Arthroplasty 29, 1681–6.
354 Lenaerts, L., van Lenthe, G.H., 2009. Multi-level patient-specific modelling of the proximal femur. A
355 promising tool to quantify the effect of osteoporosis treatment. Philos. Trans. R. Soc. A Math. Phys.
356 Eng. Sci. 367, 2079–2093. https://doi.org/10.1098/rsta.2008.0302
357 Lenthe, G. Van, de Waal Malefijt, M.C., Huiskes, R., 1997. Stress shielding after total knee replacement may
358 cause bone resorption in the distal femur. J. Bone Joint Surg. Br. 79, 117–122.
359 Lenthe, G. Van, Willems, M., Verdonschot, N., de Waal Malefijt, M., Huiskes, R., 2002. Stemmed femoral
360 knee prostheses: effects of prosthetic design and fixation on bone loss. Acta Orthop. Scand. 73, 630–
361 637.
362 Mintzer, C.M., Robertson, D.D., Rackeman, S., Ewald, F.C., Scott, R.D., Spector, M., 1990. Bone loss in the
363 distal anterior femur after total knee arthroplasty. Clin. Orthop. Relat. Res. 260, 135–43.
364 Moore D.J., Freeman M.A., Revell P.A., Bradley G.W., Tuke M., 1998. Can a total knee replacement
365 prosthesis be made entirely of polymers? J. Arthroplasty. 13, 388–95.
366 Pierre, M.A., Zurakowski, D., Nazarian, A., Hauser-Kara, D.A., Snyder, B.D., 2010. Assessment of the bilateral
367 asymmetry of human femurs based on physical, densitometric, and structural rigidity characteristics.
368 J. Biomech. 43, 2228–2236. https://doi.org/10.1007/s00210-015-1172-8.The
369 Rankin, K.E., Dickinson, A.S., Briscoe, A., Browne, M., 2016. Does a PEEK Femoral TKA Implant Preserve
370 Intact Femoral Surface Strains Compared With CoCr? A Preliminary Laboratory Study. Clin. Orthop.
371 Relat. Res. 474, 2405–2413.
372 Schroer, W., Berend, K., Lombardi, A., Lowry Barnes, C., Bolognesi, M., Berend, M., Ritter, M., Nunley, R.,
373 2013. Why are total knees failing today? Etiology of total knee revision in 2010 and 2011. J.
374 Arthroplasty 28, 116–9.
375 Seki, T., Omori, G., Koga, Y., Suzuki, Y., Ishii, Y., Takahashi, H.E., 1999. Is bone density in the distal femur
376 affected by use of cement and by femoral component design in total knee arthroplasty? J. Orthop. Sci.
377 4, 180–186.
378 Wolff, J., 1869. Uber die Bedeutung der Architektur der spongiosen Substanz. Zentralblatt für die
379 medizinische Wiss. 223–234.

Figure captions

Figure 1. Experimental setup with a) the load cell, b) planar x/y bearing, c) varus/valgus hinge (in inset), d) custom load applicator, e) painted specimen, f) ambient light source, g) focal light source, h) dual camera setup.

Figure 2. DIC region of interest surface topology on (A) the intact femur and (B) the implanted femur. The region is chosen such that the speckle patterns are visible in both trials.

Figure 3. Von Mises strain maps of all specimens for both pre- and postoperative DIC and FE measurements.

Figure 4. Von Mises surface strain distributions for both pre- and postoperative DIC and FE measurements. The strains are determined at the surface sampling points and accumulated in 500 microstrain intervals.

Figure 5. Postoperative volumetric strain energy density differences in all specimens, separated for five periprosthetic regions of interest. The SED values at each integration point in a specific ROI were multiplied by their volume and summed to yield the total strain energy per ROI.

Figure 1

Click here to access/download;Figure;Figure 1 - Experimental setup_rev.tif

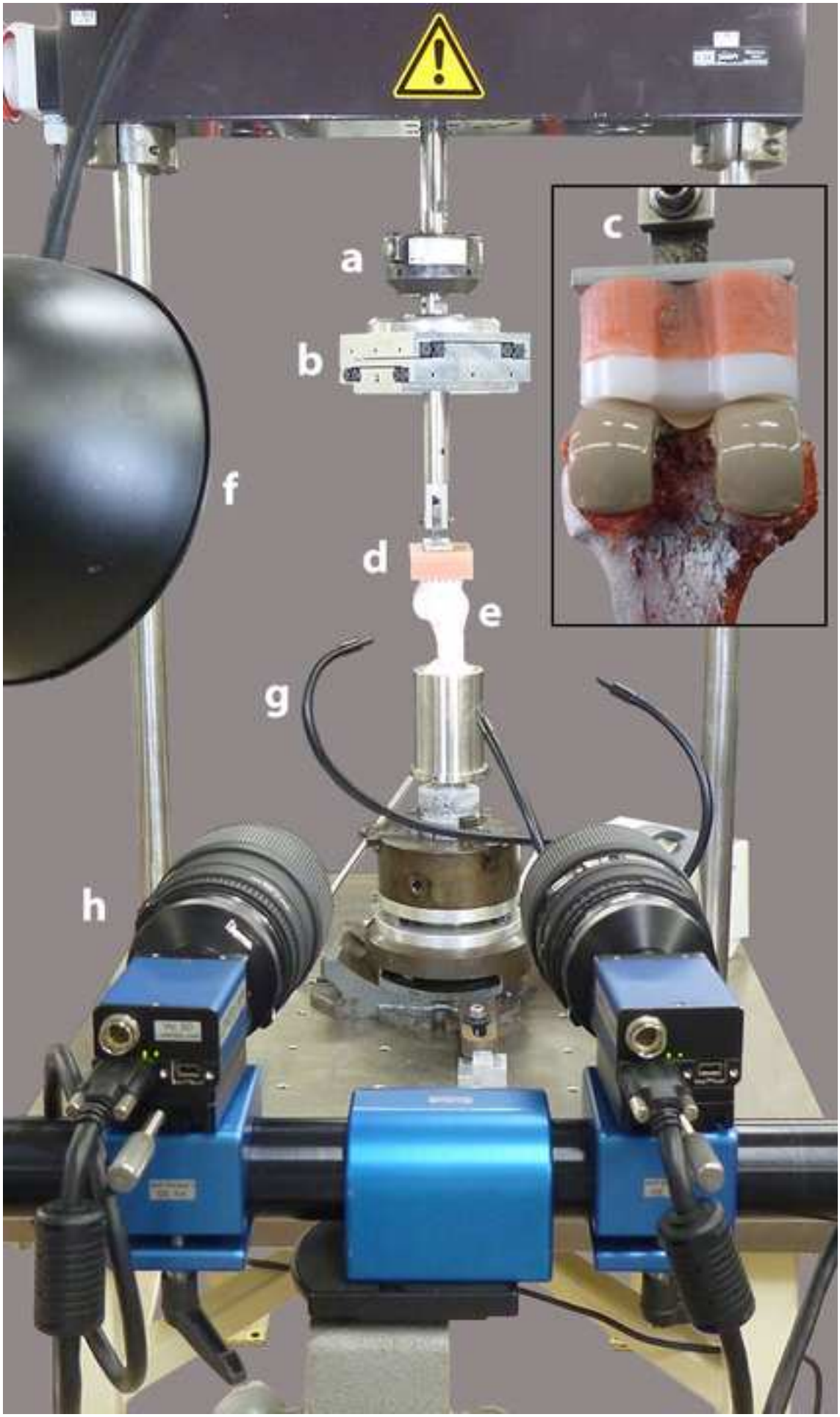

Figure 2

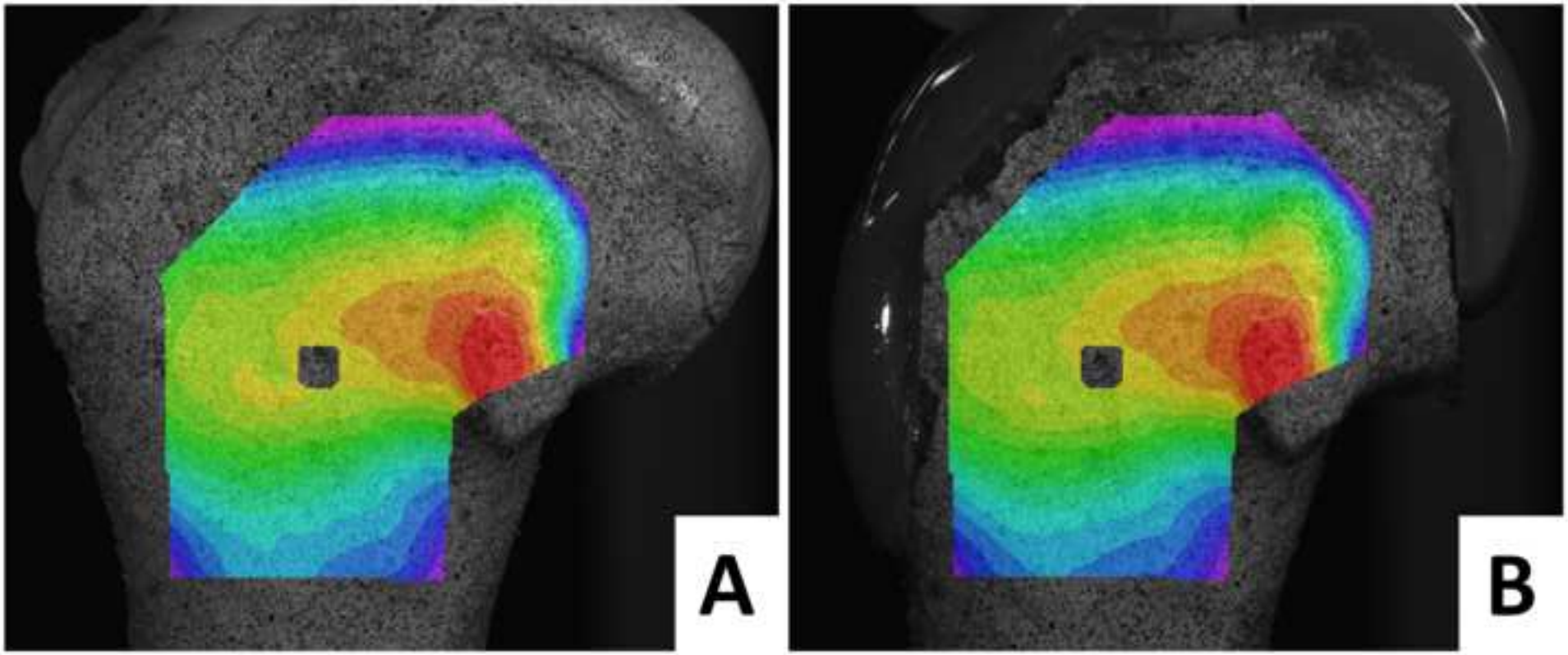

Figure 3

Click here to access/download;Figure;Figure 3 - DIC and FE data_rev.tif

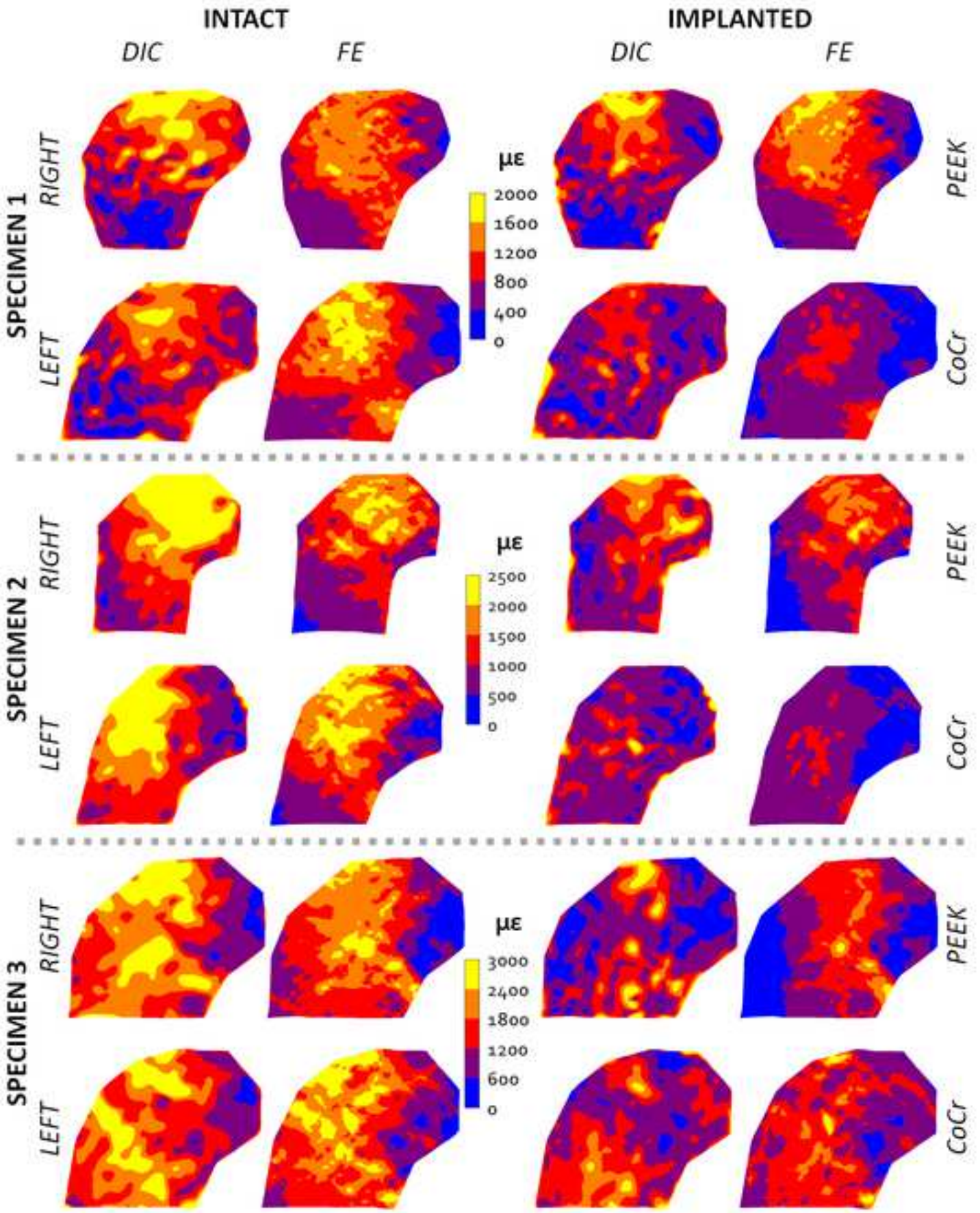

Figure 4

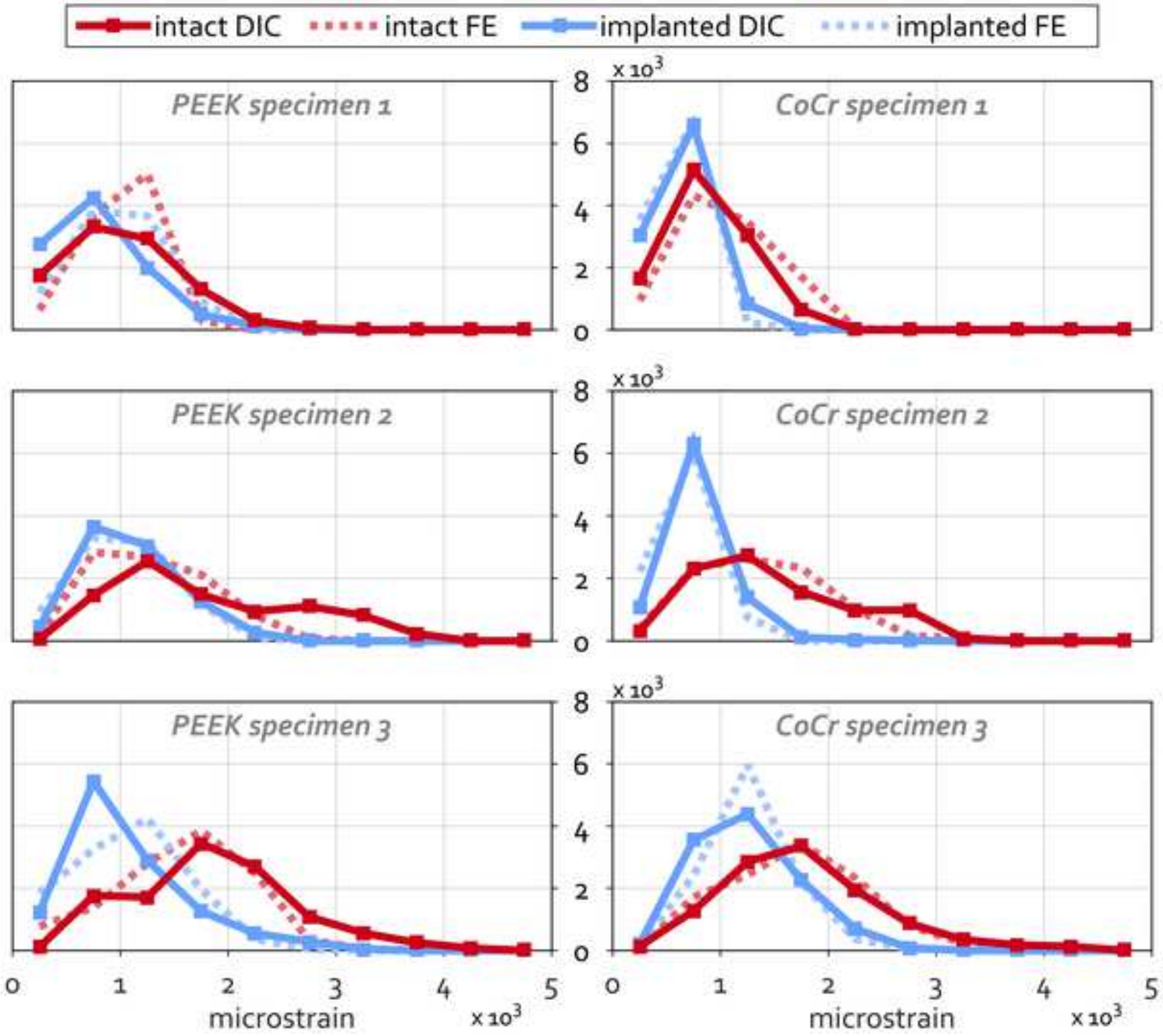

Figure 5

Click here to access/download;Figure;Figure 5 - Strain energy data - 123.tif

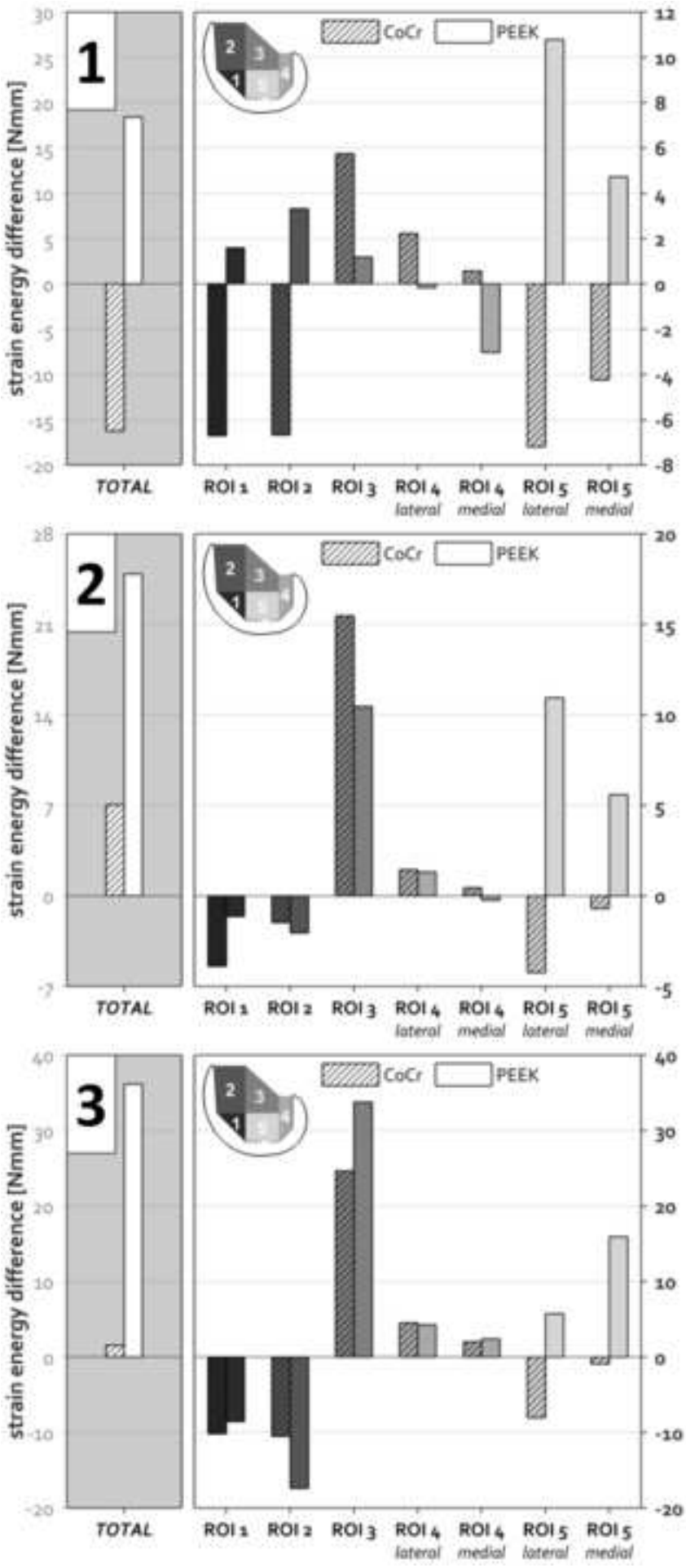

Conflict of interest statement

A.B. is a paid employee of Invibio Ltd. and had a role in the study design and review of the manuscript. M.B. has received research funding support from Invibio Ltd. N.V. is a consultant to Invibio Ltd. The other authors declare no conflict of interest. The funders had no role in the design of the study; in the collection, analyses, or interpretation of data; in the writing of the manuscript, or in the decision to publish the results.